Biophysical Journal
Article

Biophysical Society

Calcium-induced compaction and clustering of vesicles tracked with molecular resolution

Oliva Saldanha,[1] Laura Schiller,[1] and Karin Hauser[1,*]
[1]Department of Chemistry, University of Konstanz, Konstanz, Germany

ABSTRACT Theory and simulations predict the complex nature of calcium interaction with the lipid membrane. By maintaining the calcium concentrations at physiological conditions, herein we demonstrate experimentally the effect of Ca^{2+} in a minimalistic cell-like model. For this purpose, giant unilamellar vesicles (GUVs) with a neutral lipid DOPC are generated, and the ion-lipid interaction is observed with attenuated total reflection Fourier-transform infrared (ATR-FTIR) spectroscopy providing molecular resolution. Firstly, Ca^{2+} encapsulated within the vesicle binds to the phosphate head groups of the inner leaflets and triggers vesicle compaction. This is tracked by changes in vibrational modes of the lipid groups. As the calcium concentration within the GUV increases, IR intensities change indicating vesicle dehydration and lateral compression of the membrane. Secondly, by inducing a calcium gradient across the membrane up to a ratio of 1:20, interaction between several vesicles occurs as Ca^{2+} can bind to the outer leaflets leading to vesicle clustering. It is observed that larger calcium gradients induce stronger interactions. These findings with an exemplary biomimetic model reveal that divalent calcium ions not only cause local changes to the lipid packing but also have macroscopic implications to initiate vesicle-vesicle interaction.

SIGNIFICANCE The role of calcium in cellular processes is manifold. To understand the complex interaction mechanisms at cell membranes, artificial membrane systems are used to mimic biological cells. Encapsulated calcium affecting only the inner leaflet of the bilayer and calcium gradients across the membrane are both analyzed. ATR-FTIR spectroscopy enables the study of calcium-lipid interactions with molecular resolution as vibrational modes of the lipid alkyl chains, ester, and phosphate head groups monitor the calcium impact on different parts of the membrane. We propose two effects, vesicle compaction and clustering, when calcium ions interact with the membrane dependent on their location. Microscopy imaging confirms the calcium-induced membrane changes on a macromolecular scale. Our approach reveals ion-specific interactions with membranes tunable in complexity.

INTRODUCTION

Cell membranes have a need to be both dynamic yet rigid for vital molecular and biophysical function. They have to adapt and cope for processes such as membrane protrusion, fusion, foreign body-engulfment, cell signaling, and motility (1–5). For these processes to occur, calcium plays a crucial role (6–8). Calcium binding is favored by the divalent nature, and it is known that intracellular calcium concentrations are maintained at low levels from 100 nM in the cytosol up to 600 μM in the endoplasmic reticulum (9–11). Extracellular calcium concentrations are normally regulated in the mM range, at 2.2–2.6 mM and a little lower at 1.1–1.4 mM in the ionized free calcium form (12). When a cell is under stress or damage, concentrations of calcium increase and cause catalysis of downstream pathways leading the cell into an acute stress response such as exopher production (13) or even death (14). Additionally, calcium has an effect on the mechanical properties of the lipid bilayer membrane (15). It is observed that calcium ions bind to the phosphate head groups and induce conformational changes (16,17) leading to the reduction of the phospholipid area per molecule within the membrane (18). Due to calcium ion adsorption to the membrane, the surface charge density of phospholipids is found to be reduced (19). Loosely coordinated water to the membrane is released when calcium ions interact with the phosphate head groups and thus causing localized or partial dehydration (20). Membrane thickness is found to significantly increase upon calcium adsorption as well as membrane rigidity (6,21). In the cellular context, calcium ions influence the changes in membrane shape that occur during cytokinesis, which is the last step in the cell cycle (22). Furthermore,

Submitted December 22, 2022, and accepted for publication May 18, 2023.
*Correspondence: karin.hauser@uni-konstanz.de
Editor: Roland Winter.
https://doi.org/10.1016/j.bpj.2023.05.019

calcium facilitates extracellular fusion in eukaryotic cells during sperm-oocyte fusion (23) or formation of syncytia of muscle cells (24). Therefore, it is of utmost importance to understand the molecular mechanisms of calcium-membrane interaction.

Calcium effects have been studied with simplified model systems such as planar lipid bilayers for membrane rigidification in the presence of salts (6), mechanical properties (25), phase transitions, and effect of substrate hydrophilicity (26). Liposomes as another simplified model system show calcium-specific binding sites (9), membrane tubulation due to chemical gradients (27), and generation of interconnected vesicles (28). Structurally, cell membranes have a lipid bilayer of thickness ~5 nm (26), consisting of hydrophilic heads (phosphate groups) and hydrophobic tails (fatty acids). When long chain phospholipids are first dried from organic solvent and then rehydrated, they spontaneously form multilamellar bilayer sheets. Upon sonification, they are broken down into unilamellar bilayer sheets, and the ends of these bilayers seal to form a liposome or vesicles by minimizing the total surface area. In this context, giant unilamellar vesicles (GUVs) are closest to mimic biological cells in terms of size as they are in the order of ~50–120 μm in diameter, which can be generated by various laboratory techniques such as swelling (29), electroformation (30), microfluidics (31), and others.

In a GUV-based study, membrane remodeling like deformation and generation of curved tubular protrusion occur in response to calcium ions (27). Vesicles with a mixed lipid bilayer of phosphatidylcholine (PC) and phosphatidylserine (PS) are studied as a simple model of the plasma membrane because calcium ions bind naturally to negatively charged PS as shown by NMR (32,33). Vibrational sum frequency spectroscopy shows specific calcium binding sites such as the carbonyl, phosphate, and carboxylate groups of PS lipids in Langmuir monolayers (9). Complementary to this observation, molecular dynamics (MD) simulations predict lateral reorganization due to calcium ions in mixed lipid bilayers. Interestingly, recent studies in a PC/PS vesicle model show that a Ca^{2+} gradient initiates the PS lipids to flip from the outer leaflet to the inner leaflet, thereby inducing a change in the membrane curvature (34,35). The phenomenon of lipid-flipping makes mixed lipid bilayers difficult for understanding calcium gradient effects on the membrane. Hence, studies of model systems with only zwitterionic PC are favorable due to its minimalism. Such simple PC lipid models have substantial capacity for binding and clustering (6,36) since calcium primarily binds to the phosphate head in all phospholipids independent of their charge (19). Calcium not only has an effect on the membrane structure and function but can also mediate formation of GUVs with a narrow size distribution (37). A transient accumulation of Ca^{2+} polarized by an AC field occurs at the water-lipid interface and the resultant spatial-tuned electroosmotic flow leads to the homogeneous GUV population that is desirable in experiments (37).

Despite previous studies, understanding the calcium-lipid interaction with molecular resolution is still inconclusive. A sensitive analytical technique such as attenuated total reflection Fourier-transform infrared (ATR-FTIR) spectroscopy is used to detect vibrational modes of lipid groups in solution. This technique is based on the property of total internal reflection where a beam of infrared light undergoes one or several reflections through an internal reflection element (IRE). This results in the generation of an evanescent field that extends into the sample placed on the IRE surface. The penetration depth into the sample is in the range of 0.5–2 μm dependent on parameters such as wavelength, angle of incidence, and the refractive indices for the IRE and the medium being probed (38). Owing to these properties, new insights can be gained with respect to specific molecular changes occurring in a lipid bilayer in response to calcium ions (39). ATR-FTIR spectroscopy allows to detect molecular changes at physiological conditions. For this purpose, we employ a simplistic model system where GUVs are made with only PC lipids for both leaflets of the bilayer and are measured on an IRE as depicted in Fig. 1.

We demonstrate that by measuring with calcium concentrations similar to physiological ranges of ~500 μM up to 10 mM, information on calcium-binding effects at the lipid surface can be probed with ATR-FTIR spectroscopy to understand the inter- and intravesicular interaction in the presence of calcium ions.

MATERIALS AND METHODS

Lipid composition and GUV formation by electroformation

DOPC (1,2-dioleoyl-sn-glycero-3-phosphocholine, Avanti Lipids, Alabaster, USA) is dissolved in chloroform (Thermo Fisher Scientific, Belgium) at 10 mg/mL and stored at –20°C. For confocal microscopy, 1,2-dioleoyl-sn-glycero-3-phosphoethanolamin (DOPE) labeled with ATTO 488 dye is mixed with DOPC in the ratio 1:99. GUVs are formed by electroformation using a standard protocol by Angelova and Dimitrov (30) in a commercially available chamber that is temperature controlled at 37°C (Vesicle Prep pro, Nanion Technologies, Munich, Germany) and schematically shown in Fig. S1. The electroformation chamber consists of two indium tin oxide (ITO) slides, and 20 μL dissolved lipids (pure DOPC for IR studies and DOPC/DOPE-ATTO 488 for confocal microscopy) are pipetted onto the conducting side of one

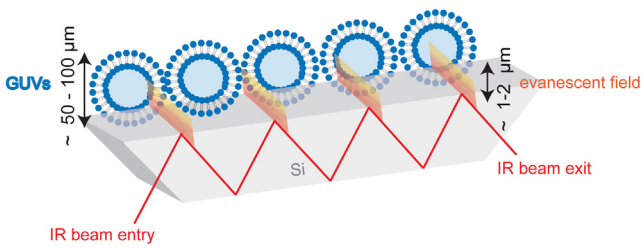

FIGURE 1 A scheme of the ATR-FTIR experimental setup (not to scale), where GUVs (Ø = ~ 50–100 μm) are measured on top of the silicon internal reflection element (IRE) with the evanescent field of the IR beam penetrating (~1–2 μm) into the sample. To see this figure in color, go online.

ITO slide and dried for 5 min to get a stack of lipid bilayers. After the chloroform evaporates, a rubber ring (d = 18 mm) is placed around the dried lipid, and silicon paste is used for sealing. 275 μL of 300 mM sucrose solution are pipetted onto it before the second ITO slide is placed with the conducting side down and screwed with a coil plate. Over time an AC field with a given frequency and amplitude runs through the ITO slides leading to hydration and swelling of the lipid bilayers. The frequency is set to 10 or 11 Hz, the amplitude between 1 and 3 V, and the formation time is between 90 and 180 min. The best vesicle homogeneity is achieved with a frequency of 10 Hz, a time of 120 min, and an amplitude of 3 V as verified by static light scattering. GUVs are harvested into 500 μL of a 250 mM glucose solution and stored for up to 2 weeks in the fridge at 4°C until measured with spectroscopy. Static light scattering is used for size characterization of lipid vesicles as seen in Fig. S2.

Sample preparation for calcium encapsulation and calcium gradient studies

For the calcium encapsulation studies, $CaCl_2$ is dissolved in 300 mM sucrose solution to reach the desired final concentration of 500 μM $CaCl_2$ and 1 μM $CaCl_2$ for the two different experiments seen in Fig. 2. The $CaCl_2$ in sucrose mixture is added to the dried lipid bilayer before electroformation starts. Once electroformation is complete, $CaCl_2$-encapsulated GUVs are harvested and stored in 250 mM glucose solution. The two sugars—sucrose and glucose—are crucial in the preparation and storage of GUVs because the osmotic concentration between the sugars is essential in maintaining membrane stability. It also allows the sucrose-filled GUVs to settle down in the glucose solution due to the molecular weight difference. For the calcium gradient studies, all experiments are performed with 500 μM $CaCl_2$ in 300 mM sucrose encapsulated in the GUVs. The gradient is achieved by externally adding a solution of the desired final concentration of $CaCl_2$ dissolved in 250 mM glucose (500 μM $CaCl_2$, 2.5 mM $CaCl_2$, 5 mM $CaCl_2$, 7.5 mM $CaCl_2$, and 10 mM $CaCl_2$) for the different experiments shown in Figs. 3 and 4. In order to verify that the vesicle membranes are impermeable to Ca^{2+} during the long acquisition times of the experiments, GUVs filled with a calcium-sensitive dye, Fluo-4 dye (Thermo Fisher Scientific, Belgium), are imaged with transmission light and confocal microscopy after 10 h. Fluorescence intensity in the interior of the GUVs with dye is not detected even after the addition of Ca^{2+} to the external solution, as seen in Fig. S3. Thus no leakage of Ca^{2+} ions is observed in the control experiments.

ATR-FTIR spectroscopy

Measurements are performed using a VERTEX 70v spectrometer and a Bio-ATR II cell (Bruker Optics, Germany). The spectrometer is equipped with a liquid nitrogen cooled mercury cadmium telluride detector. The IRE of the ATR cell is made of silicon and has 9–12 internal reflections and an incidence angle of 45°. As preparation for the measurements, the interferometer compartment of the setup is evacuated at least for ~3 h to reduce water vapor. The silicon IRE is first cleaned by incubating anionic surfactant solution of 1% SDS (sodium dodecyl sulfate) for 5 min followed by rinsing with water and isopropanol, finally polishing using a smooth cloth and Poliamant-R diamant polishing paste (Sommer, Germany). The crystal is then dried under a gentle stream of nitrogen. For the calcium encapsulation studies, 20 μL of the GUVs (for both with and without calcium ions inside) are pipetted onto the polished silicon crystal. For the calcium gradient studies, 15 μL of the 500 μM $CaCl_2$-filled GUVs are first pipetted onto the crystal. To achieve the gradient, 5 μL of the desired concentration of $CaCl_2$ dissolved in 250 mM glucose (500 μM $CaCl_2$, 2.5 mM $CaCl_2$, 5 mM $CaCl_2$, 7.5 mM $CaCl_2$, and 10 mM $CaCl_2$ for different experiments) are added on top of the GUVs. Background subtractions are done with only 250 mM glucose solution, without GUVs and without any Ca^{2+} ions. For each spectrum, 32 scans have been recorded with a resolution of 4 cm^{-1}. Data are acquired immediately after pipetting the sample onto the IRE and sealing the sample chamber. Although spectra are recorded from ~30 s onward, analysis and characterization are performed after ~5 min onward when the water vapor is reduced in the purged sample chamber.

Confocal microscopy

For visualization of the interaction of GUVs, confocal microscopy is performed on the Zeiss LSM700 microscope equipped with a light source for fluorescence excitation and laser illumination sources. Before measurements, a thin coverslip (24 × 60 mm, thickness 0.170 mm ± 0.005 mm, Paul Marienfeld & Co. KG, Germany) is prepared by washing with isopropanol and drying with a gentle stream of nitrogen. A double-adhesive spacer with a chamber diameter of 9 mm and thickness of 0.12 mm (Grace Bio-labs Secure seal, Sigma Aldrich) is placed onto the coverslip. The harvested fluorescent GUVs in glucose are pipetted onto the slide within the spacer chamber and are covered with the second coverslip finally sealing with transparent nail paint. Once dried, the sample is imaged with a 20× dry objective with a laser diode exciting at 405 nm. The images are processed with the software ZenPro (Carl Zeiss AG, Germany), and postprocessing is done with FIJI software package (ImageJ, USA).

RESULTS AND DISCUSSION

Calcium binding induces lateral vesicle compression

Biochemical studies have shown the effect of calcium in the cell cytoplasm as an essential communicator (40), but the impact of calcium on the membrane is yet to be fully understood. The lipids that make up the membrane consist of a hydrophobic (alkyl $–CH_3$/$–CH_2$) and a hydrophilic part (PO^{-2}, P-O, ester C=O), and it is important to monitor the fundamental interaction between the calcium and these lipid groups. ATR-FTIR spectroscopy is employed as a tool to track the respective lipid groups in the presence of calcium in aqueous medium. For this purpose, GUVs are first generated with calcium ions encapsulated at different concentrations, and the IR spectra are recorded between 1000 and 4000 cm^{-1}. The vibrational modes of functional groups in lipids occur in the range 900–3000 cm^{-1}, i.e., between ~1200 and 900 cm^{-1} for the phosphate head groups, between 2800 and 3000 cm^{-1} for the stretching of the alkyl groups, and at ~1453 cm^{-1} for the bending of the alkyl groups and at ~1740 cm^{-1} for the esters (41,42). The water vibrations are highly sensitive to hydration changes occurring upon calcium interaction with lipids (43) and are analyzed for hydration-dehydration effects. The three vibrational modes for water occur as symmetric stretch at ~3280 cm^{-1}, asymmetric stretch at ~3490 cm^{-1}, and bending at ~1654 cm^{-1} (44,45). As a control, IR spectra of GUVs in aqueous medium without calcium ions are recorded.

The stored GUVs are pipetted onto the IRE, and spectra shown are recorded after the sedimentation process is complete. The conditions for recording spectra are kept the same for all samples (with and without calcium). Before measuring the spectra for the GUVs, glucose in water is measured, and

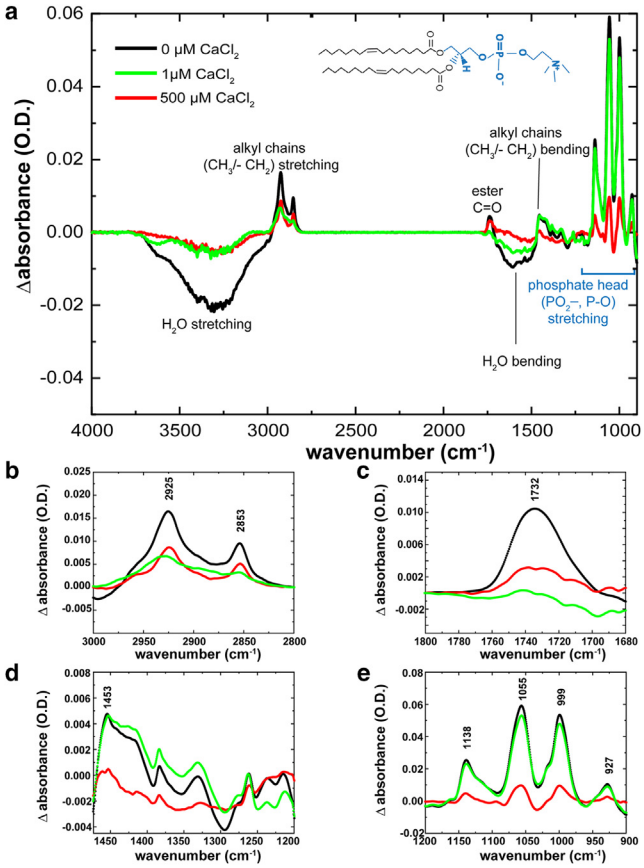

FIGURE 2 Vesicle compaction induced by Ca^{2+}. (*a*) FTIR spectra of DOPC GUVs with different calcium concentrations encapsulated within the core. (*b*) Alkyl symmetric and asymmetric stretching at 2925 and 2853 cm^{-1}. (*c*) Carbonyl stretching at 1732 cm^{-1} changes in the peak intensity for different calcium concentrations. (*d*) Alkyl bending vibrations at 1453 cm^{-1} have lower intensity for 500 μM calcium concentration. (*e*) Stretching of phosphate groups between 1200 and 900 cm^{-1}; intensities are low at higher Ca^{2+} concentrations. More calcium concentrations are shown in Fig. S5. To see this figure in color, go online.

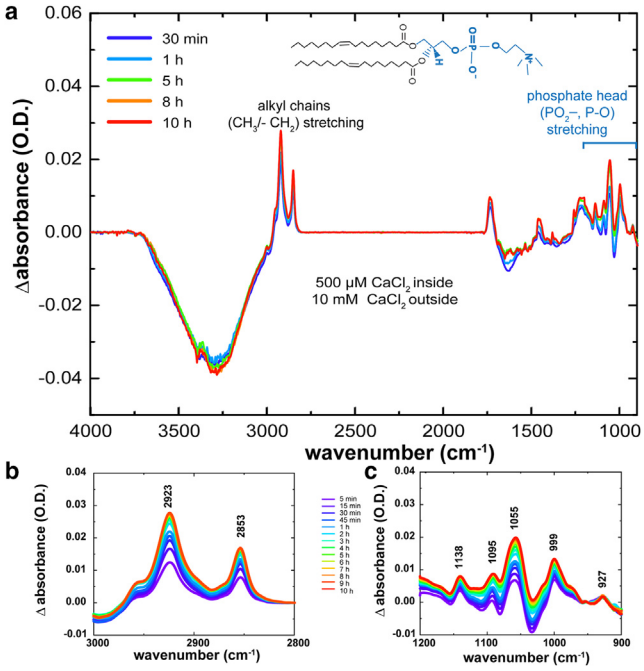

FIGURE 3 Exemplary data set of GUVs with a calcium gradient (500 μM $CaCl_2$ inside and 10 mM $CaCl_2$ outside) measured over 10 h. (*a*) Difference spectra show the vibrations of different lipid groups. A zoomed-in part of (*b*) shows the symmetric and asymmetric stretching vibrations of the alkyl groups, and (*c*) shows the symmetric stretching vibrations of the phosphate head groups. To see this figure in color, go online.

the spectrum is used as a reference. Negative water bands occur in the spectra due to the displacement of water molecules upon GUV sedimentation on the IRE surface. To ensure vesicle integrity upon contact with the IRE, control measurements are performed by intentional membrane disruption due to adding SDS on settled GUVs. Disruption of the GUVs results in positive water bands (Fig. S4) in contrast to the observed negative water bands confirming that the settled GUVs are intact. Difference spectra in Fig. 2 *a* reveal characteristic bands corresponding to the lipid groups in the GUV membrane in the presence and absence of calcium. Since there are no calcium ions in the outer medium, the interaction of ions with the lipids is only from the inside of the core of the GUVs. Therefore, the spectra show changes in the lipid groups due to the interaction of ions with just the inner leaflet, predominantly with the phosphate head and as an extension with the associated tail groups. By keeping experimental conditions the same for all samples, data recorded after sedimentation of the GUVs show negative bands for vibrational modes of water (O-H stretching and bending) in the absence of calcium. The negative water bands decrease at higher calcium concentrations. Here the calcium ions at the lipid interface have a dehydrating effect, releasing the water from inside of GUVs to the outside, causing the water band to be nearly at zero (red and green curves). Ca^{2+} is reported to induce significant gelation in the lipid bilayer possibly by dehydrating (46), and this is observed in our spectra with decrease in the negative water bands. Fig. 2 *b–e* shows selected spectral regions of the difference spectra from Fig. 2 *a*. The symmetric and asymmetric stretches of alkyl group of DOPC are shown in Fig. 2 *b*. For no calcium ions in the GUV core, the intensities of the alkyl vibrations are maximum. For calcium ions in the core, the intensities decrease as the interaction causes the chains to become rigid and ordered (20,43). A similar trend is observed for the carbonyl ester group in Fig. 2 *c*. However, for alkyl bending and phosphate head group vibrations, the intensity decreases as calcium concentration increases, as seen in Fig. 2 *d* and *e*. The GUVs with 500 μM $CaCl_2$ inside (red curve) in Fig. 2 *b–e* agree perfectly in all parts of the spectra as concentration increases and intensity decreases for the different groups of the lipid. For the GUVs with 1 μM $CaCl_2$ inside (green curve), Fig. 2 *b* and *c* shows the same effect, but in Fig. 2 *d* and *e*, it seems that the calcium concentration is not high enough to affect the lipid groups and to observe a clear effect. A systematic study with more calcium

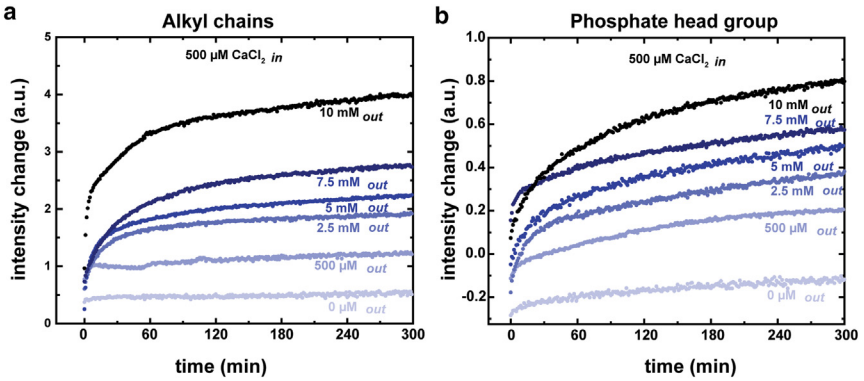

FIGURE 4 Quantification of different calcium gradients on vesicle clustering. (*a*) Integrated values of the alkyl stretches between 3000 and 2800 cm^{-1} including the peaks at 2923 and 2853 cm^{-1} are plotted up to 300 min. The different shades from light blue to black indicate the increasing calcium gradient. (*b*) Integrated values of phosphate head group stretches between 1080 and 1032 cm^{-1} including the main peak at 1055 cm^{-1} are shown for varying calcium concentrations over time. To see this figure in color, go online.

concentrations is shown in Fig. S5. The larger data set confirms that the interaction with the phosphate head groups gets stronger as the concentration of $CaCl_2$ inside the GUV increases. These measurements also indicate that at the threshold of 500 µM $CaCl_2$ inside, the binding to the phosphate head groups triggers the compaction process.

The interactions of ion-neutral lipids are governed by attractive van der Waals and repulsive hydration and steric forces (6). A change of balance is observed between the different interactions when the concentration of Ca^{2+} increases. This leads to significant ordering within a neutral lipid bilayer (POPC) in the presence of Ca^{2+} that results in a decrease of bilayer elasticity or increase in rigidity (6). The ordering occurs mainly at the alkyl chains in neutral bilayer (POPC) (20). In the context of our experiments, since the alkyl chains undergo ordering and rigidify, the intensity decreases. Calcium interaction with the lipid ester and phosphate head groups of PS-containing bilayers slows down the water dynamics at the lipid-water interface as probed by ultrafast 2D-IR spectroscopy (43).

A concentration-dependent effect is observed in the spectra of all lipid groups, the phosphate head, and the ester and alkyl chains. MD simulations suggest that each cation binds to one to four lipids (9,19,47,48). NMR studies with pure PC membranes show each cation binds to one to two lipids (49). The surface charge is neutral in PC membranes, but the surface potential is seen to increase almost linearly as the concentration of calcium increases (49). This explains concentration-dependent changes in the spectra due to cation binding seen in our DOPC-GUV model system. Deriving parallels to observations from MD simulations in PC lipids, the area per lipid is shown to decrease at higher calcium concentrations when equilibrium between bound and solvated calcium ions is achieved, thus laterally compressing the bilayer (9). Experimental observations from differential ultrasonic velocimetry show that binding of calcium ions to a PC lipid bilayer with a net neutral charge induces an increase of the average lateral pressure on the hydrocarbon region, which in turn instantaneously increases the attraction of the polar head regions, leading to bilayer compression and compaction (25). Our IR spectroscopic results agree with these findings.

The evanescent field of the IR beam penetrates about 1 μm into the sample, meaning into a section of the lipid bilayer (with a thickness of ~5 nm) of the GUV (diameters ~50–120 μm) and the aqueous core that contains the calcium ions. Therefore, any change in spectral intensity corresponds to the impact of Ca^{2+} only on the inner leaflet of this particular section of the GUV lipid bilayer as there are no ions in the outer medium. Water molecules are removed by dehydration generating a lateral compression of the phosphate head groups. The local effect seen on this bilayer section is extrapolated to the entire spherical GUV, and it is speculated that the inner leaflet of the bilayer is pulled tightly together, thus becoming more compact. The IR spectra support that Ca^{2+} primarily binds to the phosphate groups of the inner leaflet of the membrane, and further impact is seen on the ester group and alkyl chains as a consequence.

Intervesicular interactions and clustering caused by calcium gradients across the membrane

Under physiological conditions, calcium concentration in the cell cytoplasm is maintained at very low levels (50). However, up to a 10,000-fold calcium concentration gradient exists across the plasma membrane in the eukaryotic extracellular space (51), and the gradient plays an important role in cell migration (52). In order to understand the effect of the calcium gradient on the membrane, we perform further experiments by generating GUVs with 500 µM $CaCl_2$ inside and varying the concentration outside from 0 to 10 mM $CaCl_2$. In Fig. 3, an exemplary data set of GUVs with the highest Ca^{2+} gradient of 1:20 is presented (500 µM inside and 10 mM outside the lipid membrane). Difference spectra of the lipid groups are recorded from 0 to 10 h (Fig. 3 *a*). The vibrations of the alkyl chains (Fig. 3 *b*) and the phosphate head groups (Fig. 3 *c*) show an increase in intensity with time. Negative bands of O-H stretching and bending indicate the displacement of water caused by vesicles settling down on the IRE.

The vibrational mode of the alkyl chain shown in Fig. 3 *b* for an exemplary data set with a calcium gradient of 500 μM $CaCl_2$ inside and 10 mM $CaCl_2$ outside reveals a considerable change in intensity over 10 h. To quantify the change, the area under the curve between 3000 and 2800 cm^{-1} is integrated. The value obtained after integration is plotted as the first data point in Fig. 4 *a* corresponding to the first measurement set at 0 min. The integrated values for the data set in Fig. 3 *b* are plotted from 0 to 300 min and are shown in Fig. 4 *a* together with the data sets for all studied calcium gradients (500 μM $CaCl_2$ inside and 0 μM, 500 μM, 2.5 mM, 5 mM, 7.5 mM $CaCl_2$ outside). The curves for different calcium gradients show that a larger change is observed as the outer $CaCl_2$ concentration increases. Additionally, the shapes of the curves indicate that it takes longer to reach equilibrium with a higher calcium gradient. The strongest band in the spectral region 1200–900 cm^{-1} of the phosphate headgroups at 1055 cm^{-1} (Fig. 3 *c*) is analyzed the same. The less intense phosphate bands do not contribute much to the overall change in intensity. The curves are shown in Fig. 4 *b* and follow the same trend as the alkyl chains.

Further quantification of the data in Fig. 4 *a* and *b* is performed by fitting an exponential function (Fig. S6). We observe that for increasing concentration gradients, intensity changes and time constants (Table S1) increase, thereby implying that the highest change is seen for the largest difference in calcium concentration. We interpret the largest effect on vibrational modes at highest calcium gradient with the free-floating Ca^{2+} in the outer medium interacting mainly with the outer leaflets of the lipid bilayer and forming bonds with different phosphate groups of different GUVs simultaneously, thus bringing them closer together. Thereby, the observed intensity increase does not come from Ca^{2+} interactions with only one vesicle; rather, all intervesicular interactions are detected.

In order to demonstrate clustering as an effect of the calcium gradient, fluorescence confocal microscopy is performed at the same physiological concentrations as the spectroscopy experiments. In Fig. 5, the left panel shows GUVs of DOPC mixed with 1% of the dye ATTO 488-DOPE and generated by electroformation with 500 μM of $CaCl_2$ encapsulated inside and 10 mM $CaCl_2$ outside. In the left panel, the heterogeneity in the size of the GUVs arises from the electroformation production process. Optically unfocused GUVs from a different plane show up as artifacts in comparison to the focused GUVs in the selected plane. Since the image is taken immediately after the gradient is created, clustering effects are not yet observed. However, after 10 h, the same sample shows structural differences as seen in Fig. 5 (right panel). The fluorescent dye is homogenously spread in the membrane at the beginning (left panel) whereas heterogeneously accumulated in certain regions after 10 h (right panel). This indicates accumulation of lipids where the fluorescent signal is higher. Thus we observe a calcium gradient-driven clustering of the vesicles supporting the conclusions we draw from the intensity increase in the ATR-FTIR spectra and confirming the mechanism of intervesicular interaction and clustering. Without a calcium gradient, we do not observe clustering of the vesicles (Fig. S7).

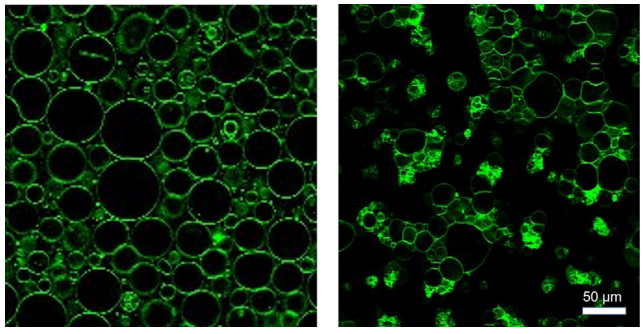

FIGURE 5 Fluorescence confocal microscopy images of GUVs with 500 μM $CaCl_2$ inside and 10 mM $CaCl_2$ outside captured immediately (left panel) and after 10 h (right panel). To see this figure in color, go online.

Proposed mechanisms of calcium-vesicle interaction

Based on our ATR-FTIR results, we conclude that there are two effects occurring at the inner leaflet of the lipid bilayer due to the calcium gradient. Firstly, the phosphate of the head group has a negative charge, and when the Ca^{2+} binds, it neutralizes this charge. This leads to the charge density difference resulting in spontaneous compaction at the monolayer in contact. Secondly, one cannot ignore the electrostatic repulsion between the calcium ions themselves which cannot diffuse as they are bound inside the vesicle due to an inward force from the bilayer. Similarly, the Ca^{2+} outside the vesicles experiences a charge density difference as a single ion can interact with the outer leaflets of two or more neighboring GUVs. Vesicle-vesicle interaction occurs, which leads to pulling the GUVs closer. It is reported that adsorption of Ca^{2+} onto PC lipid membrane applies a charge to the otherwise neutral membrane surface (53,54), and this effect can regulate interaction between bilayers (55). Not just the difference in charge density but also partial dehydration of the membrane due to Ca^{2+} binding and interaction of the polar lipid head groups with the hydration shells of the calcium ions play a role in intervesicular interaction (20). This fits well with our spectroscopic results where calcium-induced intensity changes are correlated with communication across vesicles. Our studies with other monovalent and divalent ions reveal that calcium shows the strongest effects with respect to dehydration (Fig. S8).

Despite numerous studies from ^{2}H-NMR, zeta potential measurements by particle electrophoresis, theory, and MD simulations (16,20,54,55), the determination of binding

affinity values for Ca^{2+} ions to PC lipids remains challenging. A value of 410 M^{-1} for the binding affinity of Ca^{2+} to DOPC vesicles is provided in titration experiments using an ion-selective electrode (56). Another study of DOPC lipid bilayers using tethered bilayer lipid membranes sheds light on conductance as a measure of affinity (57). It shows that as Ca^{2+} concentration increases, conductance also increases, giving a value for an apparent binding affinity of 607 M^{-1}. In our IR experiments, the spectral effects are clearly correlated with the calcium concentration and binding affinity; however, it is not straightforward to deduce an exact value. There are only a few calcium gradient studies on GUVs since the vesicles easily rupture due to concentration inhomogeneity as the ion binding affects the membrane structure. In recent years, Ali Doosti and colleagues have developed a method of inducing localized calcium gradient to the outer leaflet of the GUV by micropipetting (27). This leads to formation of membrane tubular protrusion away from the Ca^{2+} source (1,27) and generation of interconnected vesicle clusters (28). Although our membrane model is different (only DOPC lipid) compared with their mixed lipid membrane (soybean polar lipid extract and 1,2-dioleoyl-sn-glycero-3-phospho-L-serine), we can draw similar conclusions based on experimental evidence that calcium gradients across the membrane induce membrane remodeling and cluster formation. Our work indicates that these macroscopic effects on the membrane can also be observed for PC lipid vesicles.

Our observations are summarized in Fig. 6, where the left panel visualizes the effect of Ca^{2+} encapsulated in the GUVs, and the right panel shows the effect of a calcium gradient across the membrane. Ca^{2+} binding to the inner leaflet causes lateral membrane compression and dehydration, leading to GUV compaction. In addition to the compaction phenomenon and in the presence of a calcium gradient, simultaneous interaction of calcium with the outer leaflets of different vesicles occurs. Calcium-induced intervesicular interaction results in vesicle clustering.

CONCLUSION

We demonstrate that divalent calcium ions cause local and temporal changes to the lipid packing in a biomimetic cell-like model. The changes in the overall bilayer structure are reflected in the vibrational modes of the phospholipids of the membrane, thus providing molecular resolution. Our studies indicate that Ca^{2+} ions preferentially bind to the phosphate moiety of the lipid head groups. The lipid chains as a consequence also experience ordering. Ca^{2+} binding to the inner leaflet of the membrane triggers spontaneous compaction, whereas binding to the outer leaflet induces vesicle-vesicle interaction and clustering. In retrospect to our results of Ca^{2+} binding to the membrane, vesicles are more dynamic and less rigid in the absence of Ca^{2+}. Hence, this approach paves the wave to use a minimalistic model to understand the effect of any ion that alters the membrane

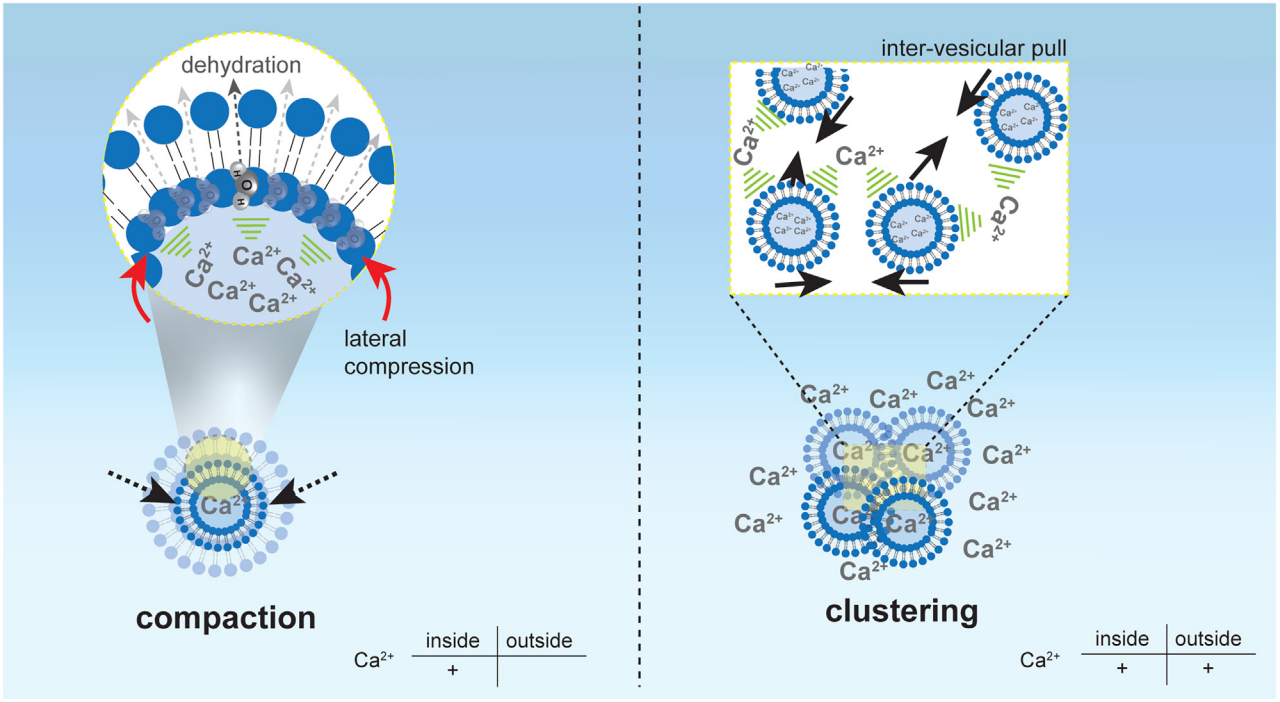

FIGURE 6 Left panel: Ca^{2+} ions, encapsulated within the core of the electroformed GUVs, interact with the inner leaflet of the vesicle and push away water molecules (between the lipid heads), leading to lateral compression, dehydration, and overall GUV compaction. Right panel: Ca^{2+} gradient between the inside and outside of the GUVs causes intervesicular interaction, resulting in vesicle clustering. To see this figure in color, go online.

properties. Moreover, various lipid mixtures with specific biological functions can be analyzed. Our studies offer the potential to track ion-specifically induced membrane modulation and derive conclusions for biological cells in vivo.

SUPPORTING MATERIAL

Supporting material can be found online at https://doi.org/10.1016/j.bpj.2023.05.019.

AUTHOR CONTRIBUTIONS

Conceptualization, O.S. and K.H.; experimental research and data analysis, O.S. and L.S.; data interpretation, O.S. and K.H., writing, review, and editing, O.S. and K.H.

ACKNOWLEDGMENTS

We gratefully acknowledge financial support by the Deutsche Forschungsgemeinschaft (SFB 1214, A3 and SFB 969, A2). We thank Dr. Martin Stöckl, Bioimaging Center, University of Konstanz for fruitful discussions on imaging.

DECLARATION OF INTERESTS

The authors declare no competing interests.

REFERENCES

1. Ali Doosti, B., W. Pezeshkian, …, T. Lobovkina. 2017. Membrane tubulation in lipid vesicles triggered by the local application of calcium ions. *Langmuir.* 33:11010–11017.
2. Aoki, K., S. Harada, …, J. Ikenouchi. 2021. STIM-Orai1 signaling regulates fluidity of cytoplasm during membrane blebbing. *Nat. Commun.* 12:480.
3. Wei, C., X. Wang, …, H. Cheng. 2012. Calcium gradients underlying cell migration. *Curr. Opin. Cell Biol.* 24:254–261.
4. Moe, A. M., A. E. Golding, and W. M. Bement. 2015. Cell healing: calcium, repair and regeneration. *Semin. Cell Dev. Biol.* 45:18–23.
5. Bharat, T. A. M., J. Malsam, …, J. A. G. Briggs. 2014. SNARE and regulatory proteins induce local membrane protrusions to prime docked vesicles for fast calcium-triggered fusion. *EMBO Rep.* 15:308–314.
6. Pabst, G., A. Hodzic, …, P. Laggner. 2007. Rigidification of neutral lipid bilayers in the presence of salts. *Biophys. J.* 93:2688–2696.
7. Monteith, G. R., D. McAndrew, …, S. J. Roberts-Thomson. 2007. Calcium and cancer: targeting Ca2+ transport. *Nat. Rev. Cancer.* 7:519–530.
8. Krebs, J. 2018. Membrane Dynamics and Calcium Signaling. Springer.
9. Melcrová, A., S. Pokorna, …, L. Cwiklik. 2016. The complex nature of calcium cation interactions with phospholipid bilayers. *Sci. Rep.* 6, 38035.
10. Xu, N., M. Francis, …, T. Stevens. 2014. Studies on the resolution of subcellular free calcium concentrations: a technological advance. *In* Focus on "Detection of Differentially Regulated Subsarcolemmal Calcium Signals Activated by Vasoactive Agonists in Rat Pulmonary Artery Smooth Muscle Cells" American Physiological Society.
11. Subedi, K. P., O. Paudel, and J. S. K. Sham. 2014. Detection of differentially regulated subsarcolemmal calcium signals activated by vasoactive agonists in rat pulmonary artery smooth muscle cells. *Am. J. Physiol. Cell Physiol.* 306:C659–C669.
12. Atchison, D. K., and W. H. Beierwaltes. 2013. The influence of extracellular and intracellular calcium on the secretion of renin. *Pflugers Arch.* 465:59–69.
13. Melentijevic, I., M. L. Toth, …, M. Driscoll. 2017. C. elegans neurons jettison protein aggregates and mitochondria under neurotoxic stress. *Nature.* 542:367–371.
14. Orrenius, S., B. Zhivotovsky, and P. Nicotera. 2003. Regulation of cell death: the calcium–apoptosis link. *Nat. Rev. Mol. Cell Biol.* 4:552–565.
15. Mitaku, S., and S. Aruga. 1982. Effect of calcium ion on the mechanical properties of lipid bilayer membrane. *Biorheology.* 19:185–196.
16. Akutsu, H., and J. Seelig. 1981. Interaction of metal ions with phosphatidylcholine bilayer membranes. *Biochemistry.* 20:7366–7373.
17. Brown, M. F., and J. Seelig. 1977. Ion-induced changes in head group conformation of lecithin bilayers. *Nature.* 269:721–723.
18. Karabaliev, M., and V. Kochev. 2004. Interaction of thin wetting films of lecithin with some divalent cations. *Bioelectrochemistry.* 63:177–181.
19. Pedersen, U. R., C. Leidy, …, G. H. Peters. 2006. The effect of calcium on the properties of charged phospholipid bilayers. *Biochim. Biophys. Acta.* 1758:573–582.
20. Binder, H., and O. Zschörnig. 2002. The effect of metal cations on the phase behavior and hydration characteristics of phospholipid membranes. *Chem. Phys. Lipids.* 115:39–61.
21. Karabaliev, M. 2007. Effects of divalent cations on the formation and structure of solid supported lipid films. *Bioelectrochemistry.* 71:54–59.
22. Atilla-Gokcumen, G. E., A. B. Castoreno, …, U. S. Eggert. 2010. Making the cut: the chemical biology of cytokinesis. *ACS Chem. Biol.* 5:79–90.
23. Wakai, T., V. Vanderheyden, and R. A. Fissore. 2011. Ca2+ signaling during mammalian fertilization: requirements, players, and adaptations. *Cold Spring Harb. Perspect. Biol.* 3, a006767.
24. Chen, W., and M. Kudryashev. 2020. Structure of RyR1 in native membranes. *EMBO Rep.* 21, e49891.
25. Aruga, S., R. Kataoka, and S. Mitaku. 1985. Interaction between Ca2+ and dipalmitoylphosphatidylcholine membranes: I. Transition anomalies of ultrasonic properties. *Biophys. Chem.* 21:265–275.
26. Regan, D., J. Williams, …, W. Langbein. 2019. Lipid bilayer thickness measured by quantitative DIC reveals phase transitions and effects of substrate hydrophilicity. *Langmuir.* 35:13805–13814.
27. Ali Doosti, B., A.-S. Cans, …, T. Lobovkina. 2018. Membrane remodeling of giant vesicles in response to localized calcium ion gradients. *J. Vis. Exp.*57789 https://doi.org/10.3791/57789.
28. Ali Doosti, B., D. Fjällborg, …, T. Lobovkina. 2020. Generation of interconnected vesicles in a liposomal cell model. *Sci. Rep.* 10, 14040.
29. Tsumoto, K., H. Matsuo, …, T. Yoshimura. 2009. Efficient formation of giant liposomes through the gentle hydration of phosphatidylcholine films doped with sugar. *Colloids Surf. B Biointerfaces.* 68:98–105.
30. Angelova, M. I., and D. S. Dimitrov. 1986. Liposome electroformation. *Faraday Discuss. Chem. Soc.* 81:303–311.
31. van Swaay, D., and A. DeMello. 2013. Microfluidic methods for forming liposomes. *Lab Chip.* 13:752–767.
32. Boettcher, J. M., R. L. Davis-Harrison, …, C. M. Rienstra. 2011. Atomic view of calcium-induced clustering of phosphatidylserine in mixed lipid bilayers. *Biochemistry.* 50:2264–2273.
33. Roux, M., and M. Bloom. 1990. Ca2 Li+, Na+, and K distributions in the headgroup region of binary membranes of phosphatidylcholine and phosphatidylserine as seen by deuterium NMR. *Biochemistry.* 29:7077–7089.
34. van Meer, G., D. R. Voelker, and G. W. Feigenson. 2008. Membrane lipids: where they are and how they behave. *Nat. Rev. Mol. Cell Biol.* 9:112–124.
35. Sun, H.-Y., G. Deng, …, Z.-W. Yu. 2017. Controllable engineering of asymmetric phosphatidylserine-containing lipid vesicles using calcium cations. *Chem. Commun.* 53:12762–12765.

36. De Mel, J. U., S. Gupta, …, G. J. Schneider. 2020. Influence of external NaCl salt on membrane rigidity of neutral DOPC vesicles. *Langmuir.* 36:9356–9367.
37. Tao, F., and P. Yang. 2015. Ca-mediated electroformation of cell-sized lipid vesicles. *Sci. Rep.* 5:9839.
38. Mirabella, F. M. 1993. Principles, theory, and practice of internal reflection spectroscopy. *In* Internal Reflection Spectroscopy-Theory and Applications CRC Press, pp. 17–52.
39. Cordomí, A., O. Edholm, and J. J. Perez. 2008. Effect of ions on a dipalmitoyl phosphatidylcholine bilayer. A molecular dynamics simulation study. *J. Phys. Chem. B.* 112:1397–1408.
40. Carafoli, E., and J. Krebs. 2016. Why calcium? How calcium became the best communicator. *J. Biol. Chem.* 291:20849–20857.
41. Fallah, M. A., H. R. Gerding, …, K. Hauser. 2017. Simultaneous IR-spectroscopic observation of α-synuclein, lipids, and solvent reveals an alternative membrane-induced oligomerization pathway. *Chembiochem.* 18:2312–2316.
42. Zhang, G., and T. A. Keiderling. 2014. Equilibrium and dynamic spectroscopic studies of the interaction of monomeric β-lactoglobulin with lipid vesicles at low pH. *Biochemistry.* 53:3079–3087.
43. Valentine, M. L., A. E. Cardenas, …, C. R. Baiz. 2018. Physiological calcium concentrations slow dynamics at the lipid-water interface. *Biophys. J.* 115:1541–1551.
44. Stomp, M., J. Huisman, …, H. C. P. Matthijs. 2007. Colorful niches of phototrophic microorganisms shaped by vibrations of the water molecule. *ISME J.* 1:271–282.
45. Goormaghtigh, E., V. Raussens, and J.-M. Ruysschaert. 1999. Attenuated total reflection infrared spectroscopy of proteins and lipids in biological membranes. *Biochim. Biophys. Acta.* 1422:105–185.
46. Kanti De, S., N. Kanwa, …, A. Chakraborty. 2018. Spectroscopic evidence for hydration and dehydration of lipid bilayers upon interaction with metal ions: a new physical insight. *Phys. Chem. Chem. Phys.* 20:14796–14807.
47. Tsai, H.-H. G., W.-X. Lai, …, W.-H. Tseng. 2012. Molecular dynamics simulation of cation–phospholipid clustering in phospholipid bilayers: possible role in stalk formation during membrane fusion. *Biochim. Biophys. Acta.* 1818:2742–2755.
48. Böckmann, R. A., and H. Grubmüller. 2004. Multistep binding of divalent cations to phospholipid bilayers: a molecular dynamics study. *Angew. Chem. Int. Ed. Engl.* 43:1021–1024.
49. Macdonald, P. M., and J. Seelig. 1987. Calcium binding to mixed phosphatidylglycerol-phosphatidylcholine bilayers as studied by deuterium nuclear magnetic resonance. *Biochemistry.* 26:1231–1240.
50. Domínguez, D. C., M. Guragain, and M. Patrauchan. 2015. Calcium binding proteins and calcium signaling in prokaryotes. *Cell Calcium.* 57:151–165.
51. Simons, T. J. B. 1988. Calcium and neuronal function. *Neurosurg. Rev.* 11:119–129.
52. Tsai, F.-C., G.-H. Kuo, …, P.-J. Tsai. 2015. Ca^{2+} signaling in cytoskeletal reorganization, cell migration, and cancer metastasis. *BioMed Res. Int.* 2015, 409245.
53. Lau, A. L., A. C. McLaughlin, …, S. G. McLaughlin. 1980. The Adsorption of Alkaline Earth Cations to Phosphatidyl Choline Bilayer Membranes: A Unique Effect of Calcium. ACS Publications.
54. McLaughlin, A., C. Grathwohl, and S. McLaughlin. 1978. The adsorption of divalent cations to phosphatidylcholine bilayer membranes. *Biochim. Biophys. Acta.* 513:338–357.
55. Szekely, O., A. Steiner, …, U. Raviv. 2011. The structure of ions and zwitterionic lipids regulates the charge of dipolar membranes. *Langmuir.* 27:7419–7438.
56. Graber, Z. T., Z. Shi, and T. Baumgart. 2017. Cations induce shape remodeling of negatively charged phospholipid membranes. *Phys. Chem. Chem. Phys.* 19:15285–15295.
57. Deplazes, E., B. D. Tafalla, …, A. Garcia. 2021. Calcium ion binding at the lipid–water interface alters the ion permeability of phospholipid bilayers. *Langmuir.* 37:14026–14033.